Electrotuneable Nanoplasmonic Liquid Mirror

Yunuen Montelongo, Debabrata Sikdar[#], Ye Ma, Alastair J. S. McIntosh, Leonora Velleman, Anthony R. Kucernak*, Joshua B. Edel*, and Alexei A. Kornyshev*

Department of Chemistry, Imperial College London, South Kensington, SW7 2AZ London, UK

Corresponding authors:
anthony@imperial.ac.uk, joshua.edel@imperial.ac.uk, a.kornyshev@imperial.ac.uk

Current Address:
[#]Department of Electronics and Electrical Engineering, Indian Institute of Technology Guwahati, Guwahati, Assam, India 781 039

Abstract

Recently, there has been a drive to design and develop fully tuneable metamaterials for applications ranging from new classes of sensors to superlenses amongst others. Although advances have been made, tuning and modulating the optical properties in real-time remains a challenge. We report on the first realization of a reversible electrotuneable liquid mirror based on voltage-controlled self-assembly/disassembly of 16nm plasmonic nanoparticles at the interface of two immiscible electrolytic solutions. We show that optical properties such as reflectivity and spectral position can be varied *in-situ* within a mere +/-0.5V. This observed effect is in excellent agreement with theoretical calculations corresponding to the change in average interparticle spacing. This electrochemical fully tunable nanoplasmonic platform can be switched from a highly reflective 'mirror' to a transmissive 'window' and back again. This study opens a route towards realization of such platforms in future micro/nanoscale electrochemical cells, enabling the creation of tunable plasmonic metamaterials.

The development of metamaterials has garnered interest ever since their initial introduction in the 19th century, leading to exploration and creation of artificial media for manipulation of electromagnetic waves. Recently, there has been a strong drive to build such media based on nanoscale bottom-up building blocks[1–3]. These have been employed to create objects with unique electromagnetic properties for applications such as antennas, absorbers in solar cells, superlenses, cloaking, sensors, etc.[4–11]. Although substantial advances have been made, tuning/modulating optical properties in real-time has remained elusive. If successful, such metamaterials would introduce dramatic change in their implications, and are expected to offer numerous new applications. For instance, energy efficient switchable windows can be designed where both the spectral range and the reflectivity can be fine-tuned. Such **t**uneable **o**ptical **m**etamaterials (**TOM**s) can also be used to circumvent limitations in trace analyte sensing, ensuring capture and detection of analytes *via* real-time tuning of the TOM.

Here we report on a step towards realizing this goal by creating an electrotuneable quasi-2-dimensional plasmonic platform: an electrically-switchable liquid mirror–window. It is based on voltage-controlled self-assembly/disassembly of negative-charge functionalized gold **n**ano**p**articles (NPs) at the **i**nterface of **t**wo **i**mmiscible **e**lectrolytic solutions (**ITIES**)[12,13]. The principle underlying its operations is as follows. At this interface NPs can be made to adsorb spontaneously, driven by capillary forces. A dense monolayer of sufficiently large gold NPs reflects light due to coupled plasmon resonance[14–18]. However, charged NPs repel each other and may not settle close enough at the interface to form a dense layer resulting in a modest reflectivity unless they are driven to aggregation and formation of a multilayer[19]. However, these systems cannot be made to spontaneously disassemble back into the liquid phase. In order to accomplish this latter aspect, the particles need to be trapped at the interface at sufficient density to form a plasmonically coupled monolayer, but not so close that they aggregate, (c.f. Figure 1a.i and iii). This is achieved by formation of a 'potential energy well' at the interface (Figure 1a.v) trapping any NP, however, electrostatic repulsion between the NPs diminishes the depth of the trapping well. Screening by electrolyte weakens the repulsion which effectively deepens the well, enabling the formation of highly reflective denser NP-arrays (Figure 1a.ii, iv and vi[20–22]). However, such 'chemical' means of tailoring of inter-NP spacing and optical reflectivity[23,24] is restricted by an upper-limit of electrolyte concentration that ensures NPs do not agglomerate in the bulk or at the interface due to Van der Waals attraction.

A 'physical', *in-situ* means of control would be possible in an electrochemical liquid | liquid cell (c.f. Figure 1b). Here, negative polarisation of the aqueous phase relative to organic phase would push the NPs towards the interface forcing NPs to tolerate the proximity of each other, increasing the density, reflectivity, while shifting the reflectance maximum towards the red end of the spectrum. Polarizing the aqueous phase positively will push NPs back into the bulk, diminishing their population at the interface, and thereby, decreasing the peak reflectivity and 'blue-shifting' it.

As mentioned, the density of the NP array at the interface can be statically controlled by the electrolyte concentration in the aqueous and organic phases and pH of the aqueous phase[24,25]. To introduce dynamic control over assembly/disassembly we need to vary the potential distribution at the ITIES. This is achieved by applying a potential difference between the electrodes in the aqueous (A) and organic (O) phases (Figure 1b), $\Delta\Phi_{AO} = \Phi_A - \Phi_O$. Under such potential bias of any polarity, two back-to-back electrical double layers will be formed on either side of the interface (Figures 1b.iii and iv). If one considers the total energy, U_{tot} , felt by a NP moving across the interface[26],

$$U_{\mathrm{tot}} = U_{\mathrm{solv}} + U_{\mathrm{cap}} + U_{\mathrm{line}} + U_{\mathrm{ext}} \quad (1)$$

comprising the free energy of transfer of a NP from aqueous to organic phase, U_{solv} (dominated by the Born resolvation energy); a capillary term including interface tensions, U_{cap}; line tension when the NP pierces the interface, U_{line}; and the electrostatic energy of the NP in the polarized electrical double layer across the interface, U_{ext}. The potential well can be made deeper by applying $\Delta\Phi_{AO} < 0$ (Figure

1b.v). Reversing the sign of $\Delta\Phi_{AO}$ makes the well shallower or can totally eliminate it, or even create a repulsive energy profile to release the NPs into the aqueous phase (Figure 1b.vi).

The principles of such electrotuneable optical platform and its main features have been proposed and theoretically investigated [20,21,26–28], however, experimentally they have not been realized. Pioneering work by Girault's group[29] first demonstrated that populations of very small NPs (<2 nm) at the ITIES can be controlled reversibly by the applied voltage. Assembly-disassembly of such NPs are relatively easy to control, but as their polarizabilities are proportional to their volume, they do not exhibit a sufficiently strong optical response required to make a mirror. However, later Girault and Brevet's group obtained signatures of reversible adsorption of larger core-shell gold-silver nanoparticles at the polarized ITIES using **s**econd-**h**armonic **g**eneration (SHG).[30] The SHG signals showed a reversible nature and an intensity controlled by the externally applied potential. But as mentioned by the authors, the observed experimental SHG intensity is "not straightforward to extract and relate to the particle surface density since the potential dependence of the adsorption isotherm is not precisely known". A recent study by Schlossman's group[31], achieved some variability in the structure of the arrays of small, 2 nm NPs. However, these particles are too small to deliver a visible optical response at the interface.[28] Dryfe's group[32] observed electrotuneable SERS with large NPs, however, continuous tuning of the inter-particle spacing and the resultant optical response of the NP-layer was not performed, nor was assembly/disassembly of the array.

In agreements with theoretical expectations[20,28], a dense interfacial assembly of large NPs, of 50-60 nm in diameter, have been shown to provide up to ~40%-50% of maximum reflectivity (even at normal incidence)[23,33] and huge Raman signal enhancements[34]. The connectivity of the assembly of 60 nm NPs, assessed through lateral conductivity measurements, has, as expected, positively affected the reflectivity[33]. However, for such systems agglomeration at the interface is almost certainly present. Furthermore for larger NPs, already not negligibly smaller than the wavelength of incident light, the corrugation of the interface becomes noticeable, contributing to light scattering. Most importantly, achieving voltage-control over the density of the layer of large NPs, from a dense monolayer to sparse submonolayer, is more challenging due to a deeper capillary well trapping such NPs at the interface, and a propensity of the nanoparticles to agglomerate.

On a historical note, the research of Yogev-Efrima's mirrors dates back 30 years.[19] Their metal like liquid films (MELLFs) can be very stable and provide strong reflectivity, but the only way to control their optical response is through their thickness or composition; in situ fine-tuning of the reflection spectra, in particular by voltage, was not possible. On solid substrates electrochemically controlled growth and dissolution of liquid metal multilayer films[35] comprises an interesting recent development.

In our paper, using functionalized gold NPs of moderate size (~16 nm in diameter), we get a strong optical response as well as its electrotuneability. We present *the first demonstration of an electrovariable liquid mirror* based on monolayer NP arrays where the *optical reflectivity of the interface* can be electrically fine-tuned *via* the voltage-controlled arrays' assembly/disassembly. These observations are directly correlated with the theoretical gap-dependent plasmonic response of such systems. The demonstrated harmony between the theory and experiments signifies again that "physics works!", something that one can never become disenthralled about.

Mercapto carboxylic acid capped gold particles and electrochemical cell configuration

Figure 2a shows a schematic of the experimental setup consisting of an electrochemical ITIES cell with an optical reflectivity probe and a four-electrode configuration. The ITIES comprises aqueous and organic [1,2-dichloroethane (1,2-DCE)] phases with 10 mM NaCl and 10 mM TBATPB (tetrabutyl ammonium tetraphenylborate), respectively. In our experiments, we utilized MDDA (12-Mercaptododecanoic acid) stabilized gold NPs with a size of 16.1 ± 1.1 nm (see Methods for synthesis details, and electrophoretic measurements). We have previously shown that 16 nm NPs

functionalized with MDDA can be used to control the average interparticle spacing at the interface over the range 6–35 nm[25]. In this work, we show that by incorporating electrovariability we can bring inter-particle distances even closer together by a factor of two (see below) making the optical effect event more dramatic. Extensive studies of the stability of these NPs were performed in order to ascertain their stability as a function of aqueous electrolyte ionic strength and non-aqueous electrolyte concentration (see SI for details). We found a limit of 37.5 mM NaCl in the aqueous solution (see Figure S12) and a limit of ca 0.1 M of TBATPB in the oil phase (Figure S13 and S14). Below these concentrations we did not see any aggregation even after extended periods (24 hours). Interestingly, it has been recently reported that for citrate- and short chain-length mercaptopropanesulfonate- stabilized gold nanoparticles, aggregation at the LLI can be induced by low concentrations of tetrabutyl ammonium cations[36,37]. We have repeated these experiments for citrate stabilized particles, finding aggregation at concentrations as low as 10^{-5} M TBATPB, and concomitant irreversible formation of aggregated Au particles at the LLI (See Figures S13 and S14). The absence of aggregation with our particles is associated with the longer chain surfactants resisting close approach of the NPs.

The ITIES was characterized by electrical capacitance (Figure 2b), obtained from impedance measured at 1 Hz frequency with 1 mV_{rms} signal amplitude, over the interval of applied voltage bias, recorded in 5 mV steps. We first checked how well the classical Verwey-Niessen theory of two back-to-back electrical double layers[38] (black dashed curve) replicates the response for bare ITIES (squares). In the range between -100 mV to +100 mV, the data reproduce theoretical predictions; outside this range, the capacitance rise is steeper. The latter has been explained by voltage-induced undulations of the interface that increase its area and thereby the capacitance[39]. The **p**otential of **z**ero **c**harge (p.z.c.) corresponds to the potential of the minimum of capacitance of the bare ITIES. With NPs at the interface (triangles) the capacitance should be larger, as when NPs pierce the interface the ITIES surface area increases[40]. We see this for $\Delta\Phi_{AO} < 0$, where NPs are pushed towards the ITIES. This effect practically disappears at $\Delta\Phi_{AO} > 0$ when NPs leave the interface for the aqueous bulk. These trends are similar to the earlier observed ones by Girault's group[41] and rationalized in Ref.[40].

Cyclic voltammograms without NPs (Figure 2c) were measured to evaluate the potential window within which no significant ionic current flows across the ITIES, c.f. SI for details. We set a target of 16 μA cm^{-2} maximum current at a scan rate of 5 mV s^{-1} to determine a safe electrochemical window at which the interface is not disturbed by ionic transport across it – as shown in SI Figure S11, at these limiting potentials the current flowing decays very rapidly during chronoamperometry and after ~3 hrs an integrated charge of less than 10 mC cm^{-2} is passed (i.e. a time-averaged current of less than 1 μA cm^{-2}). Using this criterion, we were able to sustain a 500 mV window without excessive ion transfer; all experiments described below were performed inside this range. The low average current and relatively high aqueous electrolyte conductivity mean that any static potential <<1mV, and so electrophoretic effects may be ignored.

Figure 2d shows an example of a potential energy profile for an NP at the interface under an applied voltage, based on a simplified analysis of ref[26]. One important term, in this analysis, is the Born re-solvation energy. If that model is taken literary, the barrier caused by the smeared 'Born step' for moving the NP from water into oil would cause a barrier for the NP, obstructing its entering into the interfacial well. Unlike in the graphs plotted in Ref.[26] for tiny NPs, these barriers would be too high for large NPs and not removable by the voltage variation considered in our paper. Had this been the case, NPs would have never entered the interfacial well. In reality there are effects of spatial dispersion of static dielectric response[42] ,which are expected to smear and shift the step slightly into the oil phase, and this results in disappearance of the barrier for substantial values of voltage across the interface, of the kind used in the paper. Such a shift has been implemented in plotting these exemplary curves (intended to pinpoint the possibility of such response of the interfacial well to the applied voltage for the considered values of charge of NPs).

Dynamics of assembly-disassembly of nanoparticle arrays

The theoretical estimate of the potential energy profile of a single NP at the ITIES as a function of applied voltage, shown in Figure 2d, depicts the concept of electrical modulation of the capillary well, which plays a vital role in deciding NP population at the ITIES. The curves here were calculated using the approach and equations described in detail in Ref [26], and the parameters correspond to our experimentally studied ITIES cell. The curves in Figure 2d correspond to different values of $\Delta\Phi_{AO}$; all plotted for particles of indicated size and net 871 elementary negative charges on them. Of course, one must not take this number too literally: the precise value of the charge, particularly for NP at the interface, is not known. It lies, however, within the range of a plausible estimate described in detail in the SI. Figure 2d bears only a *qualitative* message, because the theory used to plot it is too simplistic for any quantitative predictions. Furthermore, although there is a well for an individual NP at the non-polarised interface (black line), the wells will become shallower for NPs settling close to each other, when forming a dense array. To reversibly control the population of NPs at the interface with the voltage across it, we must first ensure no aggregation of NPs occur in the bulk. This can be achieved by optimizing the NP size, ligand charge/length, Debye screening, and choice of solvent. Adjustment of these parameters offers, simultaneously, a fine balance between the maximal optical reflectivity of NP arrays, and the ease of their assembly/disassembly. The theory[20,26] helps navigating the search for such conditions, but the exact system parameters has to be found experimentally, which has been achieved in the present work.

Crucially, the electric field at the ITIES is localized near the interface, within two double layers – each a Gouy-length thick[43]. At the electrolyte concentrations used, the overall width is ~4 nm. The *bulk solution will be electroneutral*, with electric field totally screened. There is no one-dimensional drift of NPs in the external field across the bulk, as the field is zero there, as expected from the near-zero current during the potential step, and the very low transference number of the gold particles in solution. Hence, the NPs will only be able to work their way to the ITIES *via random diffusion*, which imposes restrictions on the mirror switching time.

We should also ensure that the substantial $\Delta\Phi_{AO}$ is applied to avoid any potential barrier preceding the well. Under these conditions, the switch-'on'-time is determined by diffusion-controlled adsorption of NPs and can be improved by reducing the average path length via increasing the NP concentration or introducing convection. In our system, we performed experiments under temperature controlled conditions in order to minimise thermally driven convection.

Confirmation that diffusion is the predominant mode of transport is provided by the optical images of the electrolyte adjacent to the ITIES, showing a smooth and graded response over a distance of 1 cm perpendicular to the ITIES during nanoparticle absorption and desorption from the ITIES, Figure 3c. The lack of any sharp transitions and the significant distance over which the gradient is maintained strongly suggests that diffusion, and not convection, is the major transport mechanism.

Without any detailed theory, one can obtain an order of magnitude estimate for the time needed to fill the monolayer via diffusion from the bulk. The area which is expected to be occupied by one particle in a complete monolayer, $\xi\pi R^2 \equiv 1/\Gamma_{\max}$ where R is the NP radius, ξ is a packing factor with the value of the order of 1 (depending on the structure of the layer and the size of the ligands, e.g. for triangular lattice arrangement $\xi = \frac{2\sqrt{3}}{\pi}\left(1+\frac{\delta}{R}\right)$ where δ is the length of functionalizing ligands) and; $\Gamma_{\max}$ is the maximal surface coverage. Given the average concentration of NPs in the solution, an average closest distance l from such spot to any NP in the solution is estimated from equation: $c_{np} \approx \frac{1}{l\xi\pi R^2} = \frac{\Gamma_{\max}}{l}$, hence $l \approx \frac{1}{c_{np}\xi\pi R^2} = \frac{\Gamma_{\max}}{c_{np}}$. Then the time τ_a

needed for a particle to reach that spot by Brownian diffusion, would be of the order

$$\frac{l^2}{D_{np}} = \frac{1}{\left\{c_{np}\xi\pi R^2\right\}^2 D_{np}} = \left(\frac{\Gamma_{\max}}{c_{np}}\right)^2 \frac{1}{D_{np}}$$

This simple estimate gives the result close to model results. Generally, the diffusion limited dynamics of adsorption can be complicated[44], but its simplest version obeys an exact solution with

$$\tau_a = \frac{\pi}{4}\left(\frac{\Gamma_{\max}}{c_{np}}\right)^2 \frac{1}{D_{np}} \tag{2}$$

Average concentration of NPs in the bulk of the aqueous phase of our sample is estimated as 5.3 x 10^{12} cm^{-3}; for the diffusion coefficient in water of 16 nm gold NPs with 2.4 nm ligands we take for orientation the data of Ref.[45]: $D_{\mathrm{NP}} = 1.53\times10^{-7}\ \mathrm{cm^2 s^{-1}}$; for dense packing of such NPs (packing of NP centres on a triangular lattice with a lattice constant 18.8 nm, c.f. the next section), $\Gamma_{\max} = 3.26\cdot10^{11}$ particles/cm^2. From Eq.(2) we obtain then a disappointingly long time of $\tau_d = 1.93\cdot10^4\,\mathrm{s}$. As τ_d is inversely proportional to the square of concentration, the way to decrease the time is to increase concentration in the same sample. We checked this law experimentally, and the inset of Fig.3d(i), proves that $\tau_d \propto c_{np}^{-2}$ law does work.

For practical applications increasing the number of NPs is not the way to go, as this would result in stronger light absorption in the bulk solution. A way to achieve fast switching times, is to use miniaturised, micro/nano cells. For example, by using a cell with a 10 μm high aqueous layer, assembly times are expected to decrease by six orders of magnitude.

Noteworthy, as seen in Fig.3 b(iii), the dynamics of monolayer formation, after abruptly polarizing the aqueous phase negatively with respect to oil, follows the law[44] of diffusion limited adsorption. Before reaching saturation, it follows a simple diffusion law

$$\Gamma(t)/\Gamma_{\max} = \sqrt{\frac{t}{\tau_a}}, \tag{3}$$

The observed deviations from this law start only at very long times. Rahn and Hallock's extension of this law[46] reproduces both the short time behavior and saturation: $\Gamma(t)/\Gamma_{\max} = 1 - e^{-\sqrt{t/\tau_D}}$. A faster approach to 1 that we observe must be related with the ability of NPs to readjust at the interface upon accommodating new particles.

These arguments are valid when the NPs in the bulk are in substantial excess above the amount to just cover the surface. They also require the absence of the barrier for the NP at the entrance to their wells. If such barrier exists, more general equations, accounting for adsorption limitations in the adsorption kinetics[44] need to be invoked, but in our case this did not seem to be necessary. On the other hand, once the NPs are assembled at the ITIES, removing them and switching the mirror 'off' will be much faster, if the well at the interface is destroyed completely. As shown in the SI, it is sufficient for NPs to drift away from the interface some distance $l > 10R$ (R is NP-radius) in order to stop performing the coherent mirror function. The time needed for disassembly by the diffusion drift can then be estimated as:

$$\tau_{\mathrm{d}} \sim \frac{l^2}{D_{\mathrm{NP}}} \sim \frac{(10R)^2}{D_{\mathrm{NP}}} \tag{4}$$

With $R \sim 8\times10^{-7}$ cm, and again $D_{\mathrm{NP}} = 1.53\times10^{-7}\ \mathrm{cm^2 s^{-1}}$we get $\tau_{\mathrm{d}} \sim 4.2\times10^{-4}$ s. However, such value for the mirror switching-off time will be valid only if the applied potential bias fully

removes the well. However, the voltage applied is seemingly insufficient to fully remove the well, because the observed time is of the order of few seconds (c.f. Fig 3d(ii)). Where is still a metastable well separated by a barrier, the disassembly time will be determined by the Kramers time of escape from the well[47,48]. Generally, it might be interesting to describe such case, but the problem is that individual wells for NPs are affected by the presence of neighboring NPs, and once they start leaving the surface, the wells will get deeper and the process will slow down and overall will not be described by the classical Kramers model. The theory of such a complex process should be left for future research. But interestingly this is what Fig 3d(ii) exactly shows: a fast major initial stage of disassembly taking about 2s and a slower tail. This limitation can be overcome for systems with a larger potential window, as larger voltages will remove the metastable well to reach the sub-millisecond regime of disassembly.

If the wells or barriers are removed by the applied voltage, and the system is rapidly switched on and off, back-and-forth, the assembly time will be decided just by the shorter of the diffusion time and the switching interval.

Optical response during assembly/disassembly process

The results shown below demonstrate the proof-of the-principle of the electrovariable mirror–window, consistent with these estimates of the time constants. In this work, we focus on the physics of the electrovariable effect, demonstrating how it works in a macroscopic cell, unravelling the interplay between voltage-controlled assembly/disassembly and the optical response rather the working towards optimizing the response time.

Optical reflectivity of this electrovariable interface was measured with a spectrometer when illuminated by normal incidence of white unpolarised light through an optical probe. Such measured reflectance data provide typically an estimate of the minimal reflectivity from any surface. Figure 3a shows the observed evolution of the reflectivity spectra in real time after the application of -200 mV potential drop across the ITIES. This voltage induces the adsorption of NPs at the interface; the reflectance spectra evolve until the process stops. During this assembly process, the reflectance increases and its peak wavelength shifts to the red. The obtained peak reflectance R_{max} and peak wavelength λ_{max} are found to be in excellent agreement with theoretically simulated optical reflectance spectra, shown in Figures 3b.i and 3b.ii. 'Theoretical' spectra were generated using the original theory[28,24,49], under the following two assumptions.

Firstly, at steady state the NPs are considered to form a homogeneous hexagonally-ordered monolayer. In this formulation (see SI for details), we considered NPs settling right at the interface. That position can in principle vary with voltage, but this only weakly affect the calculated spectra (for discussion see SI and Figure S7). The method described in Ref [24] is then applied to find the lattice constant that matches λ_{max} of the steady-state optical reflectance spectrum (the 'long time' data). It is found that the λ_{max} at steady-state refers to a uniform monolayer with lattice constant 18.8 nm, *i.e.* shortest inter-NP, surface-to-surface, separation of 2.8 nm.

Secondly, for less dense layers it is convenient to use the approach where the filling fraction, $f = \Gamma(t)/\Gamma_{max}$ of the monolayer is varied, instead of varying the lattice constant. The fill factor $f = 1$ corresponds to a dense hexagonal monolayer in which each lattice-site would have been occupied by an NP with 100% probability. When the assembly process starts, $f \ll 1$. With time, more and more NPs adsorb at the interface, and f increases, and its optical reflectivity reaches saturation. This way we are left with just one fitting parameter f, the value of which can in principle vary between 0 and 1 to match the optical reflectance spectrum at different stages of the monolayer formation. The theoretical model for calculating optical response from an incomplete monolayer follows the same strategy as applied for the complete monolayer. The only difference would be in the effective polarizability expressions, which are affected by the value of f (the corresponding derivations are presented in the SI). With this new approach, we can find the fill factors that match the reflectance maximum R_{max} and

peak wavelength λ_{max} at every time point of the assembly process. As expected and already mentioned, the fill factor evolution follows a diffusion limited adsorption law (Eq.(2)), up to the times close to the saturation (as shown in Figure 3b.iii), with the diffusion coefficient of NPs of the value of 1.53×10^{-7} cm^2/s Ref.[45]

The spatial density distribution of NPs in the solution adjacent to the ITIES can be clearly observed from the side windows of the cell. Figure 3c shows the schematic and actual photographs (colour gradient panels) corresponding to the NP density distribution in the aqueous phase during assembly (i) and disassembly (ii), each after a period of 4 hours.

Evolution of the reflectance peak R_{max} during assembly and disassembly of NPs for two different concentrations are shown in Figure 3d. According to Eq. 3, the speed of assembly increases quadratically with the concentration of NPs (Figure 3d.i). The insert in Figure 3d.i shows data for experiments performed at three concentrations, which clearly demonstrates the $\tau_a \propto n^{-2}$ law. The disassembly process is practically independent of concentration, c.f. Eq. 4 (Figure 3d.ii).

Electrotuning of the optical metasurface

A clear advantage of an electroactive TOM is in the ability to fine tune the reflectivity spectrum, including peak reflectance, R_{max}, and peak wavelength, λ_{max}, by changing the applied potential. Figure 4a shows the time-dependence of R_{max} and λ_{max} during the disassembly process. In this experiment, first a monolayer was formed at $\Delta\Phi_{AO}$ = -250 mV, then the potential was increased to the p.z.c. until the spectra stabilized. Noticeably within the first 30 s the system attained a constant reflectivity, although λ_{max} takes a little longer to stabilize (~100s).

In Figure 4b the equilibrium reflectance spectra are shown, as well as the theoretically calculated ones, for a series of potentials between -250 to 250 mV. In the calculated spectra, for each potential, the adopted lattice constant (NP-surface-to-surface separation) in the NP hexagonal array was different, subjected to the best fit to the measured spectra; Figures 4c.i and 4c.ii show fits being in excellent agreement. Fig.4c.iii shows the dependence of the thus obtained inter-NP separation on voltage; as expected for large negative $\Delta\Phi_{AO}$, a dense monolayer is formed with short inter-NP separation. For less negative voltages the potential well that keeps NPs at the interface becomes less deep, which makes it harder for them to tolerate their mutual electrostatic repulsion, so some NPs will have to leave the interface. As a result, the inter-NP separations increase and the reflectance diminishes, vanishing at large positive potentials.

The variation of inter-NP separation as a function of applied voltage demonstrates the proof-of-concept for a 'voltage-controlled plasmon ruler'. It allows us to tune inter-NP separation over a range of about 3–20 nm *in-situ* just by altering the applied potential $\Delta\Phi_{AO}$ within a 500 mV window.

Tuning the NP array structure can also be performed consecutively. After inducing the complete assembly at -250 mV we further conducted a multi-step disassembly process (Figure 4d) with the potential $\Delta\Phi_{AO}$ increased in 50 mV steps, from -250 mV to 250 mV. Each potential step had a duration of 1000 seconds. These experiments once more show that the interparticle distance can be precisely controlled which allows accurate tuning of both reflectance intensity and peak wavelength.

Reversibility of the electrotuneable device

Switching the liquid-mirror 'on' (applying $\Delta\Phi_{AO}$= -200 mV) and 'off' ($\Delta\Phi_{AO}$= 200 mV) for two consecutive cycles demonstrates the full reversibility of the designed TOM (Figure 5a.i–iv). We fabricated a prototype device (Figure 5b) of a switchable window–mirror, which can be altered electrovariably between its transmissive and reflective states. To demonstrate this, we placed a coin in front of the liquid mirror and a currency note at the back of the mirror, as shown in the schematic Figure 5c.

The transformation from a 'window' to a 'mirror' is shown in Figure 5d (see also the supplementary video). A positive applied potential made the ITIES free of NPs and hence, the interface emulated a transmissive 'window' that allows us to see the currency note. After reversing the voltage polarity, NPs gradually adsorb to the interface and form a dense layer that behaves like a reflective 'mirror'. The reflection of the coin can thus be seen. The reflectance response for four consecutive cycles can be seen in the section on repeatability in the SI and Figure S11.

Conclusion

Here we present the first realization of an electrochemical nanoplasmonic platform operating with medium size NPs that provides electrotuneable optical responses. In this platform, we reversibly control the interparticle distances in two dimensional arrays of NPs at a liquid-liquid interface, from full assembly to disassembly and back, by varying the potential drop across the interface. This allows us to control the wavelength-dependent reflectivity of the interface. We demonstrated that different potentials produce, correspondingly, different steady-state reflection spectra. The peak reflectance was tailorable both in intensity and wavelength. We show how this system can be used to fabricate a switchable window–mirror device.

The dynamics of the operation is dictated by the diffusion of NPs to/from a polarized liquid | liquid interface. We observe that the assembly time is inversely proportional to the square of the concentration of NPs, as expected from a diffusion driven assembly process. The disassembly time is independent of NP concentration. In a macroscopic electrochemical cell, used in this proof-of-the-principle investigation, the dynamics of assembly is slow determined by diffusion of NPs over, on average, long distances. The dynamics can be sped up by orders of magnitude via miniaturization of the cell.

Experimental results are corroborated by theoretical predictions, demonstrating the simple physics behind the voltage controlled assembly-disassembly of NPs is correct, as well as our ability to calculate the reflection spectra from NP arrays using transparent, simple theory. This study opens up a wide range of possibilities for designing electrotuneable optical metamaterials including switchable mirrors, filters, displays and SERS sensors.

Methods

Synthesis of MDDA functionalized gold NPs

Briefly, 500 mL $HAuCl_4$ (0.01 wt%, > 99.9% purity) solution was heated to boiling with continuous stirring, followed by addition of 10 mL sodium citrate (1 wt%, > 99.0% purity). The solution turned from yellow to dark blue then finally to red within 10 min and was kept boiling for a further 30 min. The temperature was cooled down to 60 °C, then 25 mg MDDA (12-Mercaptododecanoic acid, 96% purity) were added and kept at that temperature for 2 hours. The solution was then cooled to 4 °C in order to precipitate excess MDDA. This method produced an aqueous NP solution with a measured concentration of 1.09×10^{12} NPs/cm^3. Samples of the Au-MDDA NPs were drop cast from solution onto a TEM carbon grid (JEOL 2100 PLUS) (Figure S1.a). The final NP size was 16.1 ± 1.1 nm, analysed using image processing software (Figure S1.b). The absorbance of the bulk solution was analysed with a UV-Vis spectrometer (Nanodrop 2000, thermo scientific) to check for agglomeration which presents as a shoulder at high wavelength (Figure S1.c).

Concentration of NPs

The final concentration of NPs was controlled through centrifugation. The solution was placed in two 50 mL tubes in an Eppendorf 5430 centrifuge at 6000 rpm for 1 h. After centrifugation, 45 mL of the excess water was removed from the total 50 mL. The concentrated solution was re-dispersed with water to obtain the desired concentrations.

Electrochemical cell

To prepare the solutions for the electrochemical ITIES cell, 40 mL of aqueous solution (with 10 mM NaCl, >99% purity) and 75 mL of DCE (>99% purity) solution with 10 mM tetrabutylammonium tetraphenylborate (TBATPB, 99.0% purity) were mixed by convection to accelerate reaching the equilibrium

state. The prepared ITIES is positioned in an electrochemical cell as shown in Figure 2a. Typically, the system took approximately 15 min to fully stabilize. The concentration of NPs in the aqueous phase was carefully controlled to ensure the total number of NPs was greater than the amount needed to fully assemble a close-packed monolayer which equates to 3.18×10^{11} NPs/cm^2 for 16 nm NPs. Briefly, the cell dimension had a cross-sectional area of 26 cm^2 and the height of the aqueous solution L was 1.5 cm. The electrochemical setup contained four electrodes. Two platinum electrodes were used as working and counter electrodes for aqueous and organic phases respectively. The working and counter electrodes have platinum rings attached to distribute the electric field homogeneously in the cell and were positioned at 1 cm from the interface. The sense and reference electrodes consisted of Ag-AgCl wires inside capillaries located at a 2 mm distance from the interface in the aqueous and organic phase respectively. Particularly, the reference was not in direct contact with DCE and a separated aqueous phase with 10 mM of tetrabutylammonium chloride (TBACl, 98% purity) was added to reduce impedance. The potential in the rest of the manuscript refers to the aqueous phase with respect to the reference in the organic phase.

Optical reflectivity measurements

An Ocean Optics reflection probe with a focal length of 2.25 mm was used to measure reflectance and consists of an optical fibre bundle that deliver light and a single multimode fibre that collect light. The white light source utilized was a Tungsten Halogen lamp and the signal was collected using an Andor 163 spectrograph fitted with an iDus CCD. The reference reflection was obtained from an aluminium mirror. The spectrometer was programmed through the AndorBasic language to perform consecutive measurements until steady spectra were achieved (integration time, etc.). The reflection measurements were synchronized with the Gamry potentiostat software. The absorbance of NPs in the bulk solution, present in the path of light between the optical probe and the mirror, was measured. This was utilized to compensate for any loss of reflected light in the path between the probe and ITIES.

Data availability. The data that support the findings of this study are available from the corresponding author upon request.

Additional Information
Supplementary information (SI) accompanies this paper at http://www.nature.com/nmat

It contains: (i) Details on characterization of functionalized gold NPs including zeta potential measurements; (ii) estimation of net charge on NP; (iii) three-phase contact angle data; (iv) the model for extraction of capacitance from impedance data; (v) principles, and equations of the theoretical model for the analysis of the adsorption-desorption dynamics through reflectivity spectra; (vi) parameters of optical response of gold; (vii) estimation of the mirror switch off time; (viii) four cycle reversibility and current transients; (ix) characterization of the stability of Au NPs.

References

1. Fan, J. A. *et al.* Self-assembled plasmonic panoparticle clusters. *Science* **328,** 1135–1138 (2010).
2. Stebe, K. J., Lewandowski, E. & Ghosh, M. Oriented assembly of metamaterials. *Science* **325,** 159–160 (2009).
3. Nie, Z., Petukhova, A. & Kumacheva, E. Properties and emerging applications of self-assembled structures made from inorganic nanoparticles. *Nat. Nanotechnol.* **5,** 15–25 (2010).
4. Lal, S., Link, S. & Halas, N. J. Nano-optics from sensing to waveguiding. *Nat. Photonics* **1,** 641–648 (2007).
5. Engheta, N. Circuits with light at nanoscales: optical nanocircuits inspired by metamaterials. *Science* **317,** 1698–1702 (2007).
6. Kabashin, A. V. *et al.* Plasmonic nanorod metamaterials for biosensing. *Nat. Mater.* **8,** 867–871 (2009).
7. Kawata, S., Inouye, Y. & Verma, P. Plasmonics for near-field nano-imaging and superlensing. *Nat. Photonics* **3,** 388–394 (2009).
8. Shalaev, V. M. Optical negative-index metamaterials. *Nat. Photonics* **1,** 41–48 (2007).
9. Maier, S. A. *et al.* Plasmonics—A route to nanoscale optical devices. *Adv. Mater.* **13,** 1501–1505 (2001).

10. Atwater, H. A. & Polman, A. Plasmonics for improved photovoltaic devices. *Nat. Mater.* **9,** 205–213 (2010).
11. Willets, K. A. & Van Duyne, R. P. Localized surface plasmon resonance spectroscopy and sensing. *Annu. Rev. Phys. Chem.* **58,** 267–297 (2007).
12. Samec, Z. Electrical double layer at the interface between two immiscible electrolyte solutions. *Chem. Rev.* **88,** 617–632 (1988).
13. Samec, Z. Electrochemistry at the interface between two immiscible electrolyte solutions. *PURE Appl. Chem.* **76,** 2147–2180 (2004).
14. Jensen, T. R., Schatz, G. C. & Van Duyne, R. P. Nanosphere lithography: Surface plasmon resonance spectrum of a periodic array of silver nanoparticles by ultraviolet−visible extinction spectroscopy and electrodynamic modeling. *J. Phys. Chem. B* **103,** 2394–2401 (1999).
15. Jain, P. K., Huang, W. & El-Sayed, M. A. On the universal scaling behavior of the distance decay of plasmon coupling in metal nanoparticle pairs: A plasmon ruler equation. *Nano Lett.* **7,** 2080–2088 (2007).
16. Ghosh, S. K. & Pal, T. Interparticle coupling effect on the surface plasmon resonance of gold nanoparticles: from theory to applications. *Chem. Rev.* **107,** 4797–4862 (2007).
17. Su, K.-H. *et al.* Interparticle coupling effects on plasmon resonances of nanogold particles. *Nano Lett.* **3,** 1087–1090 (2003).
18. Halas, N. J., Lal, S., Chang, W.-S., Link, S. & Nordlander, P. Plasmons in strongly coupled metallic nanostructures. *Chem. Rev.* **111,** 3913–3961 (2011).
19. Yogev, D. & Efrima, S. Novel silver metal liquidlike films. *J. Phys. Chem.* **92,** 5754–5760 (1988).
20. Flatté, M. E., Kornyshev, A. A. & Urbakh, M. Electrovariable nanoplasmonics and self-assembling smart mirrors. *J. Phys. Chem. C* **114,** 1735–1747 (2010).
21. Edel, J. B., Kornyshev, A. A., Kucernak, A. R. & Urbakh, M. Fundamentals and applications of self-assembled plasmonic nanoparticles at interfaces. *Chem. Soc. Rev.* **45,** 1581–1596 (2016).
22. Booth, S. G. & Dryfe, R. A. W. Assembly of nanoscale objects at the liquid/liquid interface. *J. Phys. Chem. C* **119,** 23295–23309 (2015).
23. Smirnov, E., Peljo, P., Scanlon, M. D., Gumy, F. & Girault, H. H. Self-healing gold mirrors and filters at liquid–liquid interfaces. *Nanoscale* **8,** 7723–7737 (2016).
24. Velleman, L. *et al.* Tuneable 2D self-assembly of plasmonic nanoparticles at liquid|liquid interfaces. *Nanoscale* **8,** 19229–19241 (2016).
25. Turek, V. A. *et al.* Plasmonic ruler at the liquid–liquid interface. *ACS Nano* **6,** 7789–7799 (2012).
26. Flatté, M. E., Kornyshev, A. A. & Urbakh, M. Understanding voltage-induced localization of nanoparticles at a liquid–liquid interface. *J. Phys. Condens. Matter* **20,** 073102 (2008).
27. Edel, J. B., Kornyshev, A. A. & Urbakh, M. Self-assembly of nanoparticle arrays for use as mirrors, sensors, and antennas. *ACS Nano* **7,** 9526–9532 (2013).
28. Sikdar, D. & Kornyshev, A. A. Theory of tailorable optical response of two-dimensional arrays of plasmonic nanoparticles at dielectric interfaces. *Sci. Rep.* **6,** 33712 (2016).
29. Su, B. *et al.* Reversible voltage-induced assembly of Au nanoparticles at liquid|liquid interfaces. *J. Am. Chem. Soc.* **126,** 915–919 (2004).
30. Abid, J.-P., Abid, M., Bauer, C., Girault, H. H. & Brevet, P.-F. Controlled reversible adsorption of core−shell metallic nanoparticles at the polarized water/1,2-dichloroethane interface investigated by optical second-harmonic generation. *J. Phys. Chem. C* **111,** 8849–8855 (2007).
31. Bera, M. K. *et al.* Interfacial localization and voltage-tunable arrays of charged nanoparticles. *Nano Lett.* **14,** 6816–6822 (2014).
32. Booth, S. G., Cowcher, D. P., Goodacre, R. & Dryfe, R. A. W. Electrochemical modulation of SERS at the liquid/liquid interface. *Chem. Commun.* **50,** 4482–4484 (2014).
33. Fang, P.-P. *et al.* Conductive gold nanoparticle mirrors at liquid/liquid interfaces. *ACS Nano* **7,** 9241–9248 (2013).
34. Kondrat, S., Wu, P., Qiao, R. & Kornyshev, A. A. Accelerating charging dynamics in subnanometre pores. *Nat. Mater.* **13,** 387–393 (2014).
35. Park, C. *et al.* Switchable silver mirrors with long memory effects. *Chem. Sci.* **6,** 596–602 (2015).

36. Konrad, M. P., Doherty, A. P. & Bell, S. E. J. Stable and Uniform SERS Signals from Self-Assembled Two-Dimensional Interfacial Arrays of Optically Coupled Ag Nanoparticles. *Anal. Chem.* **85,** 6783–6789 (2013).
37. Xu, Y., Konrad, M. P., Lee, W. W. Y., Ye, Z. & Bell, S. E. J. A Method for Promoting Assembly of Metallic and Nonmetallic Nanoparticles into Interfacial Monolayer Films. *Nano Lett.* **16,** 5255–5260 (2016).
38. Verwey, E. J. W. & Niessen, K. F. XL. The electrical double layer at the interface of two liquids. *Lond. Edinb. Dublin Philos. Mag. J. Sci.* **28,** 435–446 (1939).
39. Daikhin, L. I., Kornyshev, A. A. & Urbakh, M. Capillary waves at soft electrified interfaces. *J. Electroanal. Chem.* **483,** 68–80 (2000).
40. Marinescu, M., Urbakh, M. & A. Kornyshev, A. Voltage-dependent capacitance of metallic nanoparticles at a liquid/liquid interface. *Phys. Chem. Chem. Phys.* **14,** 1371–1380 (2012).
41. Younan, N., Hojeij, M., Ribeaucourt, L. & Girault, H. H. Electrochemical properties of gold nanoparticles assembly at polarised liquid|liquid interfaces. *Electrochem. Commun.* **12,** 912–915 (2010).
42. Kornyshev, A. A. Nonlocal screening of ions in a structurized polar liquid — new aspects of solvent description in electrolyte theory. *Electrochimica Acta* **26,** 1–20 (1981).
43. Girault, H. H. & Schiffrin, D. H. in *Electroanalytical Chemistry* (ed. Bard, A. J.) **15,** 1 (CRC Press, 1988).
44. Miura, T. & Seki, K. Diffusion influenced adsorption kinetics. *J. Phys. Chem. B* **119,** 10954–10961 (2015).
45. Wong, K., Chen, C., Wei, K., Roy, V. a. L. & Chathoth, S. M. Diffusion of gold nanoparticles in toluene and water as seen by dynamic light scattering. *J. Nanoparticle Res.* **17,** 153 (2015).
46. Rahn, J. R. & Hallock, R. B. Antibody binding to antigen-coated substrates studied with surface slasmon oscillations. *Langmuir* **11,** 650–654 (1995).
47. Kramers, H. A. Brownian motion in a field of force and the diffusion model of chemical reactions. *Physica* **7,** 284–304 (1940).
48. Hanggi, P. Escape from a metastable state. *J. Stat. Phys.* **42,** 105–148 (1986).
49. Sikdar, D., Hasan, S. B., Urbakh, M., Edel, J. B. & Kornyshev, A. A. Unravelling the optical responses of nanoplasmonic mirror-on-mirror metamaterials. *Phys. Chem. Chem. Phys.* **18,** 20486–20498 (2016).
50. Volkov, A. G., Deamer, D. W., Tanelian, D. L. & Markin, V. S. Electrical double layers at the oil/water interface. *Prog. Surf. Sci.* **53,** 1–134 (1996).

Acknowledgements

The authors thank F.Bresme, A. Fedosyuk D.J. O'Lee, G. Oshanin and O. Robothan for useful discussions. The work was majorly supported by the grant of the Engineering and Physical Sciences Research Council UK, "Electrotuneable Molecular Alarm", EP/L02098X/1. JBE also acknowledges receipt of ERC starting (NanoP) and consolidator grants (NanoPD).

Author Contributions

Y.M. obtained all data for optical and electrochemical measurements, D.S. carried out all theoretical calculations in feed-back mode with experiments; Y.M. and D.S. treated the data, M. Y. and L.V. participated in preparation of NPs, A.M. helped in building the electrochemical setup. AAK, A.R.K., and J.B.E. designed the work and supervised the project, A.A.K., J.B.E., D.S., ARK, and Y.M. analysed the results and wrote the paper.

Competing financial interests: The authors declare no competing financial interests.

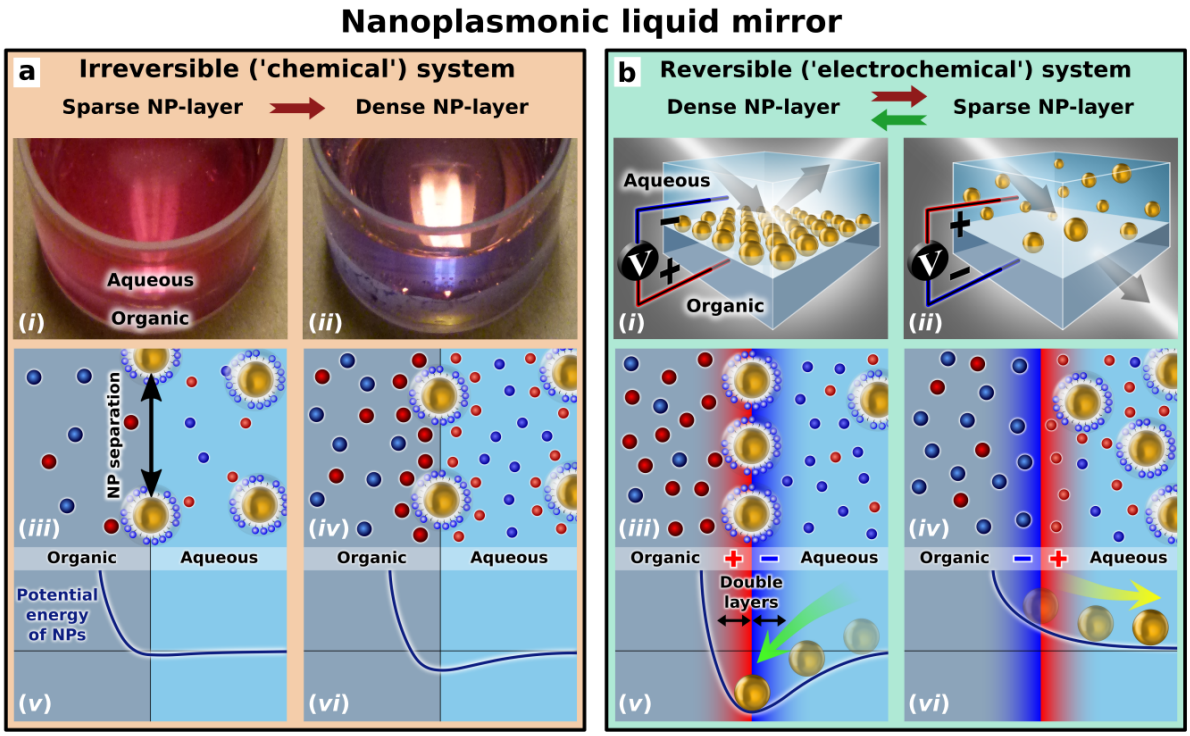

Figure 1. **Nanoplasmonic liquid mirror strategies**. a, Spontaneous adsorption of NPs at the interface between aqueous and organic phases can be controlled by the concentration of electrolytes in either phases to transform a sparse NP layer into a dense layer, making it more reflective, as seen in photographs (i) and (ii). Increased concentration of electrolytes reduces electrostatic repulsion between NPs, functionalized by negatively charged ligands, allowing formation of denser layers, as shown in the cartoon (iii) to (iv). Cations, anions, and NPs, are depicted here as red, blue, and gold spheres, respectively (all sizes are not in scale, but in proper order). (v) to (vi) depict the change in the potential energy well for NPs at the interface, which gets deeper when the electrostatic repulsion between the NPs is reduced with the increase of electrolyte concentration. **b,** Placing the system in an electrochemical cell would allow to reversibly control the assembly (adsorption) to and disassembly (desorption) of NPs from the interface by changing the polarity of the applied potential drop across the interface. This way the NP layer can be made even denser than that formed by the spontaneous assembly in the same system, or can be completely removed from the interface, as shown in schematics (i) to (ii), and (iii) to (iv). Two back-to-back electrical double layers form at the polarized interface, making the potential well for NPs deeper (v) or shallower (vi), subjected to the sign of the applied voltage. Such electrotuneable nanoplasmonic liquid mirror can thus be reversibly turned ‘on’ and ‘off’.

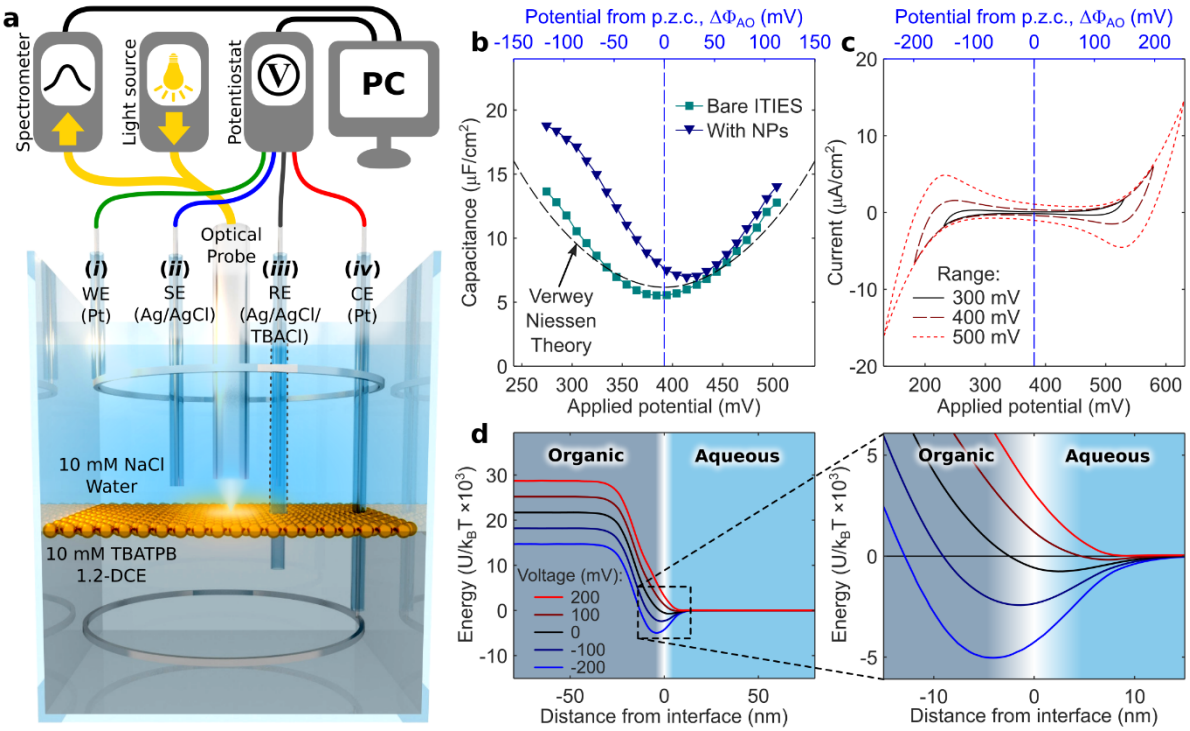

Figure 2 **Electrochemical setup and characterization. a,** Schematic of the ITIES electrochemical cell with an optical probe. The probe shines light onto the interface and transports reflected light to the spectrometer. The potentiostat is connected to the cell through (i) working (WE) and (ii) sense (SE) electrodes in aqueous phase, and (iii) reference (RE) and (iv) counter (CE) electrodes in organic phase. All electrodes are protected with glass capillaries; WE and CE have ring terminals. **b,** Capacitances of bare ITIES (■) and with NPs (▲) in the aqueous phase, $5x10^{12}$ cm^{-3}. Adsorption of NPs at ITIES increases the capacitance at negative $\Delta\Phi_{AO}$ [40]. The bottom, black dashed curve corresponds to Verwey–Niessen (Gouy-Chapman) theory of two back-to-back electrical double layers (without NPs) plotted for the used electrolyte concentrations and solvents[50]. The minimum of U-shaped capacitance of a bare ITIES is taken as the potential of zero charge (p.z.c.). **c,** Cyclic voltammograms recorded at 5 mV/s over different voltage ranges showing the limits within which there is negligible ionic current across the interface. **d,** Calculated potential energy profile of a single NP at the ITIES containing 10 mM TBA-TPB 1,2-DCE and 10 mM NaCl in water, controlled by applied voltage. The blow up highlights the stabilization of the well at negative polarization and its elimination by positive polarization. Curves in (d) are plotted using the equations of Ref.[26] for NP radius of 8 nm, an example charge of -871e (estimates in SI suggest that its value lies in the range of 900±50 – see SI for details), and a three-phase contact angle experimentally determined to be 112^{o} – see SI.

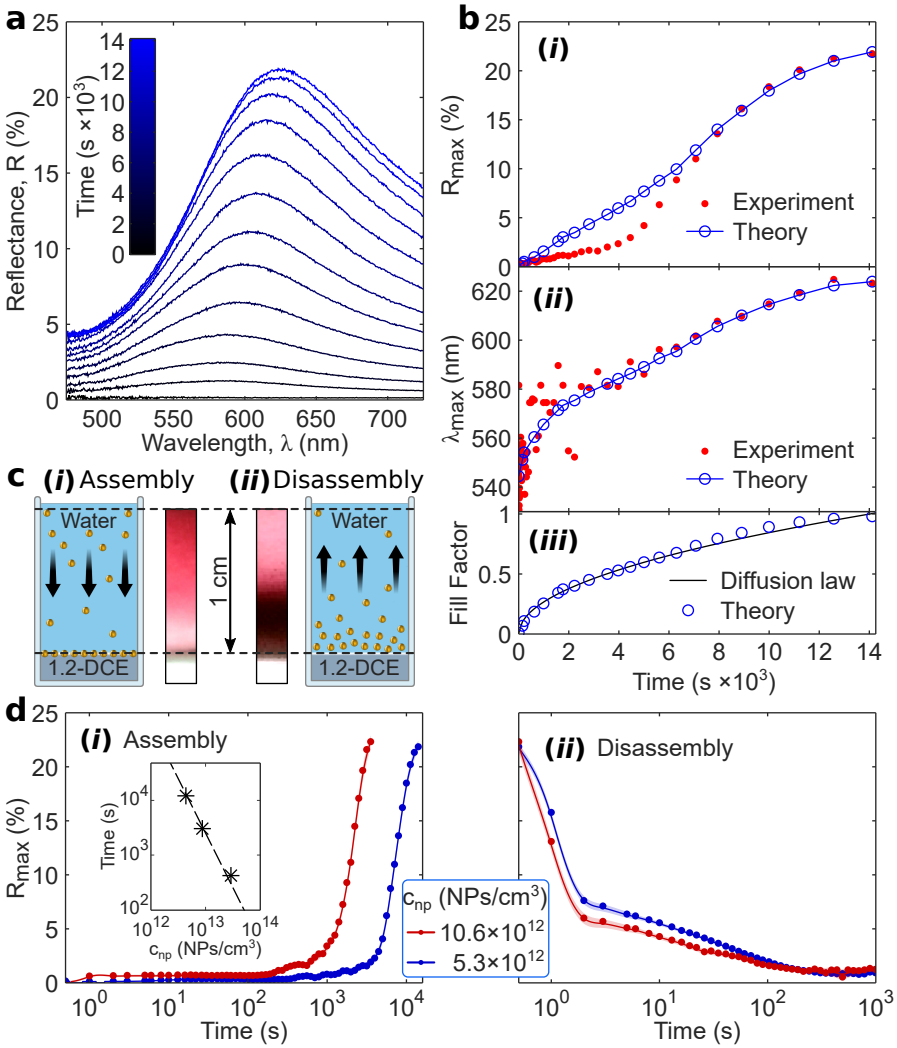

Figure 3 **Dynamics of assembly and disassembly of 16nm diameter MDDA functionalised gold NPs at the ITIES interface**. **a,** Optical reflectance spectra observed during assembly process in equally spaced time steps ranging from 1 to 14116 seconds at the potential bias -200 mV (water relative to oil). **b,** The peak reflectance R_{max} (i) and peak wavelength λ_{max} (ii) measured during the assembly process (red filled circles) are compared against their theoretical estimates (blue open circles connected by a line). (iii) The time dependence of the fill factors – the coverage of the interface by NPs (blue open circles) obtained from theoretical fitting are then compared against those obtained from the diffusion-limited adsorption (Eq.(3)) law (solid black curve), with a fitted value of the diffusion coefficient, eventually coinciding with$1.53\text{x}10^{-7}$ cm^2/s reported in Ref.[45] and the bulk NP concentration c_{np}=$5.3\text{x}10^{12}$ NP/cm^3. **c**, Cartoons of assembly (i) and (ii) disassembly process 'viewed' from the side of the container; the middle colour gradients are real photographs of the same view taken during the experiment, with the ITIES at the bottom of the images. The latter correspond to density distributions of NPs in the aqueous phase during (i) assembly and (ii) disassembly after a period of 4 hours **d,** Evolution of reflectance peak R_{max} during assembly (i) and disassembly (ii) of NPs for two different concentrations. The potential applied for assembly was -200 mV and for disassembly 200 mV. The scaling of the adsorption time as $1/n^2$ is well seen in the insert of (i) plotted for three concentrations of NPs – $5.3\text{x}10^{12}$, $10.6\text{x}10^{12}$, and $35.4\text{x}10^{12}$ NPs/cm^3. ITIES: 10 mM NaCl aqueous /1,2-DCE + 10 mM TBATPB organic phases.

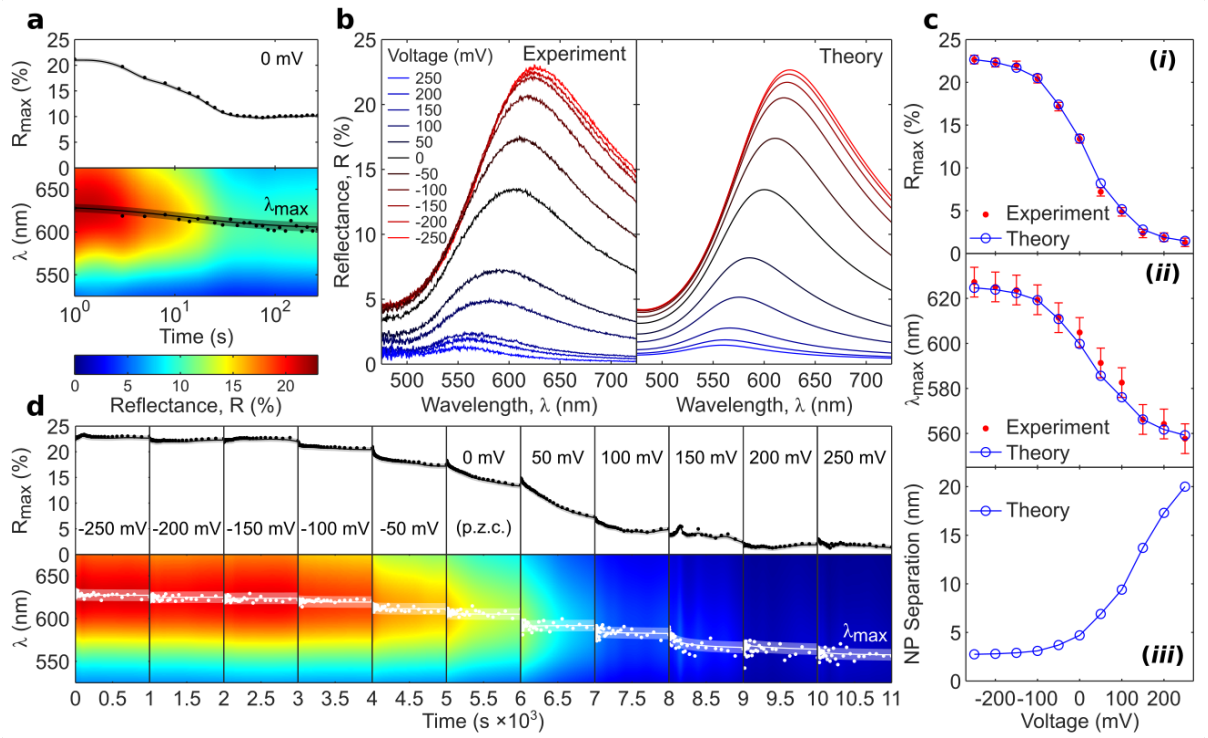

Figure 4 **Voltage-controlled plasmon ruler utilising 16nm diameter MDDA functionalised gold NPs at the ITIES interface. a,** Evolution of peak reflectance R_{max} and peak wavelength λ_{max} of the NP mirror. The experiment was conducted in a two-step process: first, the NP mirror was assembled at a negative polarization (-250 mV) of the aqueous phase relative to the oil phase. Then the potential was increased to the p.z.c. and kept such for 200 seconds, the spectra were recorded until they stabilize. **b,** Optical reflectance spectra were recorded at steady-state for different applied electric potentials: experimental (left panel) and theoretical (right panel). **c,** Comparison between the experimental data (red circles) and theoretical calculations (blue open circles connected by a line) for (i) R_{max} and (ii) λ_{max} for different applied potentials; (iii) shows variation of the inter-NP separation, fitted for the theory to reproduce the experimental reflectance spectra, with applied voltage. **d,** Steady states observed when the NP mirror was disassembling in a multi-step process, starting from a fully assembled layer to a state when the majority of NPs leave the interface. Each step, corresponded to indicated voltage, lasted 1000 seconds after which the spectra stabilized. ITIES: 10 mM NaCl aqueous /1,2-DCE + 10 mM TBATPB organic phases.

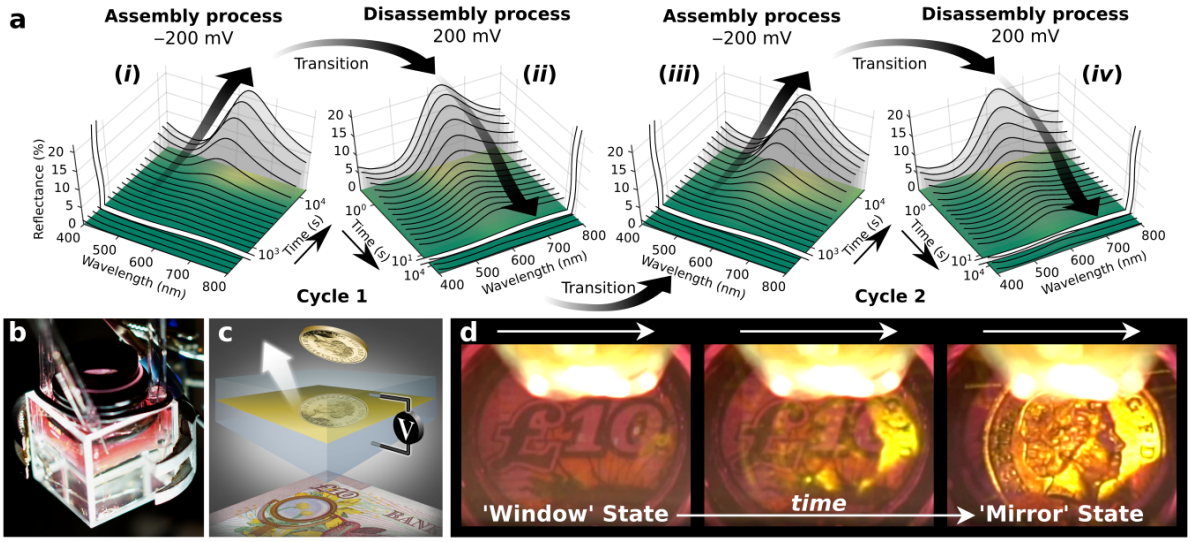

Figure 5 **Switchable window–mirror. a,** Time dependent study showing two cycles of reversible spectral characteristics of a mirror/window application where NPs (i) assemble at -200 mV and(ii) disassemble at 200 mV, followed by a repetition of those two states in a consecutive cycle – (iii) and (iv). **b,** Experimental setup for recording switchable liquid window–mirror application. **c,** Schematic showing the setup with a coin facing the liquid mirror and a currency note at the back of the mirror. **d,** Real images observed during the transition between a transmissive 'window' state (when no NPs are at the interface) to a reflective 'mirror' state (when NPs assemble densely at the interface); for a corresponding video see SI. 16nm diameter MDDA functionalised gold NPs at the ITIES interface which was composed of a 10 mM NaCl aqueous /1,2-DCE + 10 mM TBATPB organic phase interface.